



---

## ENGINEERING DESIGN REPORT

---



**Team Name:** INFERNO DTU  
DELHI TECHNOLOGICAL UNIVERSITY

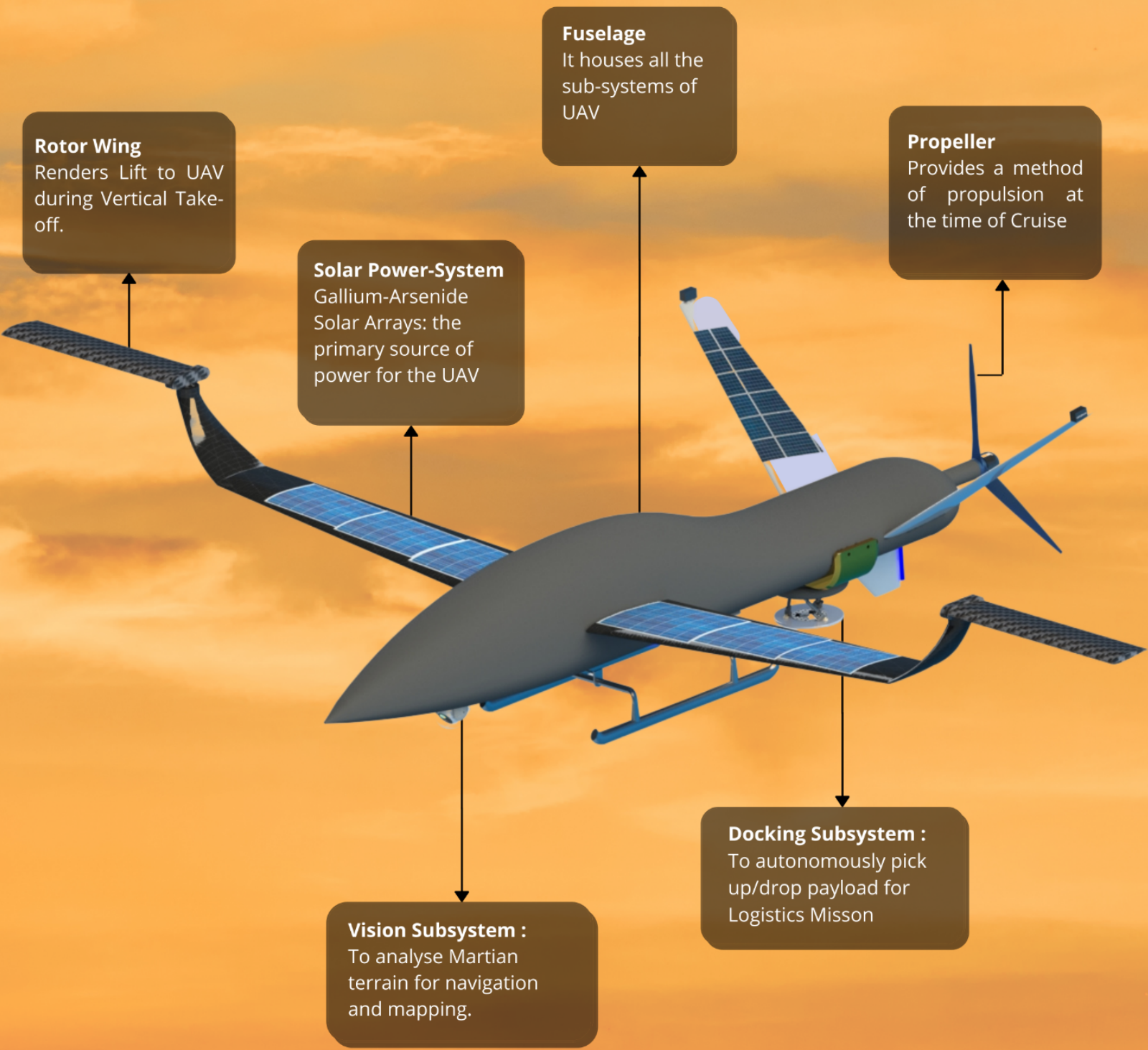


---

**Team Lead:** Daksh Jain

**E-mail:** teaminferno@dtu.ac.in

# AVYAKT



## Abstract:

An Unmanned Aerial Vehicle for Mars exploration designed by Inferno DTU to compete in the International Planetary Aerial Systems Challenge organised by the Mars Society South Asia. The objective is to design a UAV that can explore Mars and is to be controlled and monitored within a 5 kilometres range from a base station on Mars itself. The UAV has been designed to comply with all the requirements of the challenge while taking Mars and its environmental specifications into consideration. The team conducted a thorough investigation to design a UAV capable of withstanding extra-terrestrial conditions.

Contents	Page No.
Mission Architecture	4
Selection Category of UAV	4
Design Process	5
UAV Mechanics <ul style="list-style-type: none"> <li>▪ Aircraft Geometry</li> <li>▪ Fuselage</li> <li>▪ Airfoil Selection</li> <li>▪ Morphed Wing</li> <li>▪ UAV Morphing Plan</li> <li>▪ Tail Selection</li> <li>▪ Propeller Design</li> </ul>	5
Payload Carrying Mechanism	9
Weight Distribution	10
Environmental Control	11
Power System	12
UAV Electronics <ul style="list-style-type: none"> <li>▪ CPU</li> <li>▪ Flight Controller</li> <li>▪ Motors</li> <li>▪ Modes of Operation</li> <li>▪ Microcontroller</li> </ul>	14
Vision System	17
Communication System	17
UAV Software	17
Pre-flight System Check	20
UAV Science Package <ul style="list-style-type: none"> <li>▪ Planetary Surface Analyser (PSA)</li> <li>▪ Carolic Imaging Spectrometer (CIS)</li> <li>▪ Atmospheric Data Systems (ADS)</li> <li>▪ Infrared Spectral Chemistry Suite (ISCS)</li> <li>▪ High-Precision Neutron Detector (HPND)</li> <li>▪ Sub-surface Sounding RADAR &amp; Altimeter (SSRA)</li> <li>▪ MAGNM Magnetometer</li> </ul>	21
References	27

## Mission Architecture:

**AVYAKT** mission requires traversal over a 10 km planned path from a vantage point 8-10 km above the surface of the terrain. During traversal measurement and sampling of both the Martian atmosphere and terrain would be carried out using the science cache onboard. Apart from this, it would also transport a payload from the base station to the desired location within a radius of 5 km and then return back to the base station.

Extensive trade studies and design cycles were performed to develop a low-risk mission architecture. The resultant architecture as shown in Fig 1 enabled the satisfaction of the mission requirements through a simple low-risk flight system design.

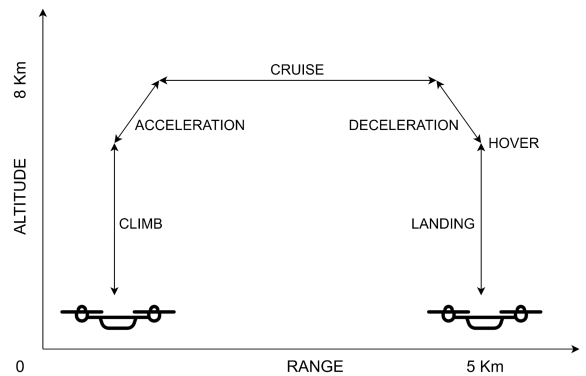


Fig:1 Mission Architecture

## Selection of Category of UAV:

Based on the evaluations given below we decided to design a fixed-wing hybrid UAV capable of performing VTOL (**V**ertical **T**ake-**O**ff and **L**anding), hence making it suitable to carry out the operation on Mars.

Weightage	Selection Criteria	Single Rotor	Multi Rotor	Fixed Wing	Fixed Wing Hybrid
10	Compactness	10	8	5	6
10	Reliability	5	7	9	9
10	Simplicity of Structure	8	7	7	6
9	Payload Packaging	4	6	9	9
8	Controllability	4	6	8	8
8	Maturity of Technology	10	8	9	8
8	Hover Efficiency	8	10	0	10
8	VTOL	9	10	0	10
8	Simplicity of Control Systems	8	7	9	7
7	Cruise Efficiency	7	6	9	9
6	Aerodynamic Cleanliness	8	7	8	7
3	Aerodynamic Interaction	7	8	8	9
3	Maneuverability	5	7	8	7
<b>TOTAL</b>		<b>711</b>	<b>731</b>	<b>658</b>	<b>788</b>

Table 1: Trade off study between various systems

## Design Process:

A systematic design approach has been used to design our UAV. The constraints have been analyzed first followed by the selection of airfoils for both wing and tail. A preliminary design of the fuselage, wing and tail has been developed based on calculations and analysis which has been refined to minimize weight and optimize storage. The final design has undergone several analyses to ensure whether or not the design is adept enough to fly in the challenging martian atmosphere. **Structural and Thermal analysis** have been carried out to prevent any kind of mechanical failure during operations.

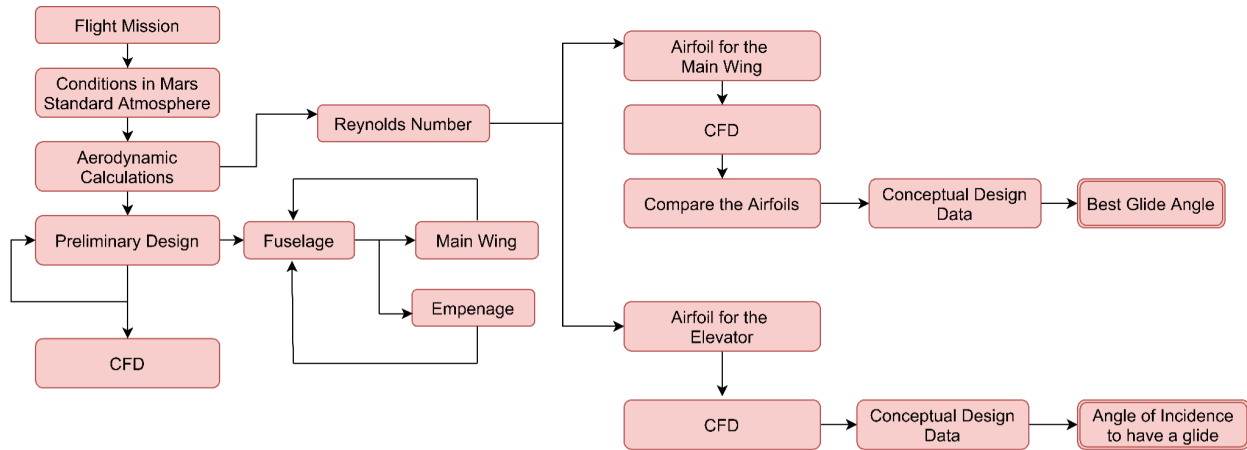


Fig 2: Design Plan

## UAV Mechanics:

All the materials used for parts have been decided after optimization using various criterions like weight, hardness, yield strength, tensile strength etc. Owing to the property of gold to block radiation, the parts of the UAV have been **gold plated** to protect the UAV from extreme levels of UV Radiations. After considerable research and studying various options, **gear lubrication has** been insured by a mixture of 50 percent 802EP grease and 50 percent 815Z oil to maintain efficiency even at extremely low temperatures as these lubricants do not dry out easily. For lubricating other components such as bearings, motors, etc.; penzane-3 Pb Np oil and 601 EF have been formulated from PFPE oil which has been thickened from PTFE powder are used [1].

The aerodynamic and structural analysis of the UAV has been done considering several factors and the calculations have been made considering the weight of the UAV to be 10 Kgs on Mars.

## Aircraft Geometry:

Our plan has mixed the drifting capacity of a helicopter and rapidly expanded perseverance flying of a fixed-wing airplane. This has helped our UAV to gain the benefits of both into one. It is based on the basic principles of the DOS SAMARA concept [2].

We have used outboard wing panels that are 1 m long and have a root and a tip chord of 0.3m, that spin to generate thrust to lift the UAV in vertical flight. The wings rotate at 3000 RPM generating a maximum lift of 110N making them capable of lifting the UAV from ground. Both rotors rotate in opposite directions hence generating a contour torque preventing the UAV

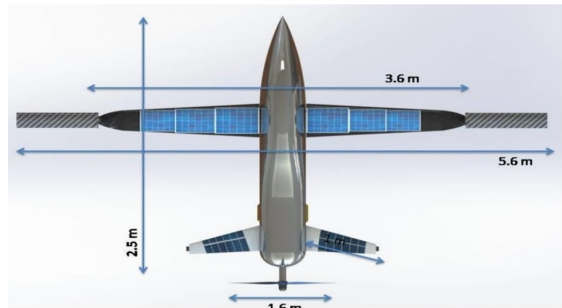


Fig 3 : UAV Dimensions

from spinning. During horizontal translation the outboard wing panels lock hence, acting as a fixed-wing. A pusher propeller is located aft of the UAV to provide thrust during the cruise. For deciding the wing geometry, possible planform shapes have been explored extensively, several trade studies between wing area and aspect ratio have been performed and the theoretical location of the wing aerodynamic center

has also been constrained to avoid large deviations of the required aircraft center of gravity. Based on the outcome of these studies, a baseline planform with an aspect ratio of 17.4 and a wing area of  $1.8\text{m}^2$  has been selected.



Fig 4 : Side view of UAV

structure making it capable of landing comfortably on uneven martian terrain.

### Fuselage:

The Fuselage is an integral part of the UAV. It has been designed to maximize storage capacity while minimizing the weight. The fuselage houses the Flight Electronics, Science Module, and everything that has to be incorporated in or on the UAV. The Fuselage is **1.5 m long and about 0.6 m wide** making it adept to cache all the components appropriately, enabling a compact and efficient design. The Fuselage has been fabricated using **Mylar and AS Graphite-Epoxy composite<sup>[3]</sup>**. This material provides an excellent strength-to-weight ratio and could easily withstand both temperature extremes on Mars.

Ease of Serviceability has been kept in mind while designing all the components making all subsystems accessible to the astronaut during maintenance. Openings have been provided both under the fuselage as well as on the rear end which makes it easier to access the electronics without dismantling the wings.

### Airfoil Selection:

Several Airfoils including Eppler 203, NACA 66(3)-418, RG-15<sup>[4]</sup>, i.e those capable of operating under Low Reynolds Number and High Mach Number(0.6-0.8) on martian atmosphere have been considered and after performing extensive analysis of those airfoils considering various key factors such as density, pressure, gravity etc RG-15 has been selected for our design. The airfoil provides a **minimum drag coefficient as well as a maximum lift coefficient**, which means the highest lift-to-drag ratio, also it

provides a low pitching moment coefficient.

These characteristics empower our UAV wing with noteworthy thrust and negligible drag, subsequently diminishing the power consumption and force utilization for an efficient flight. The airfoil which has been selected for our UAV guarantees a positive Coefficient of Pressure enabling us to

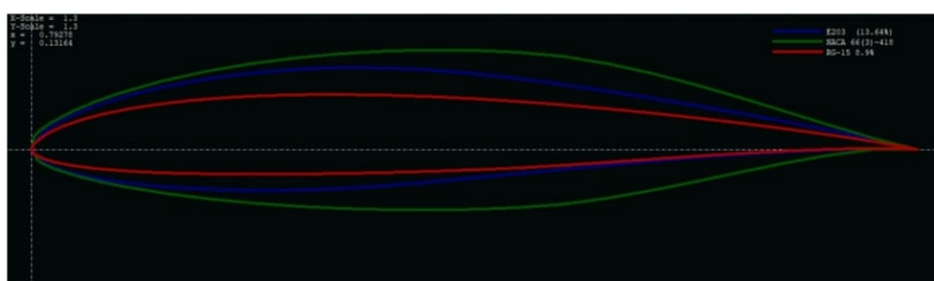


Fig 5 : Comparison between airfoils (E203,NACA 66(3)-418,RG-15)

achieve a Lift Coefficient as high as possible. An angle of attack of 8 deg. has increased the aerodynamic force and has streamlined power, along with giving a positive moment about the Aerodynamic Center.

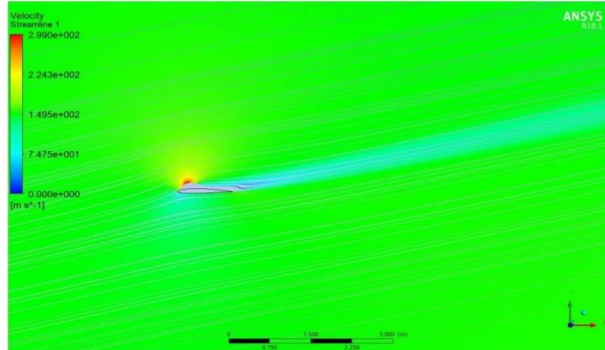


Fig 6 : Velocity Magnitude (RG15)

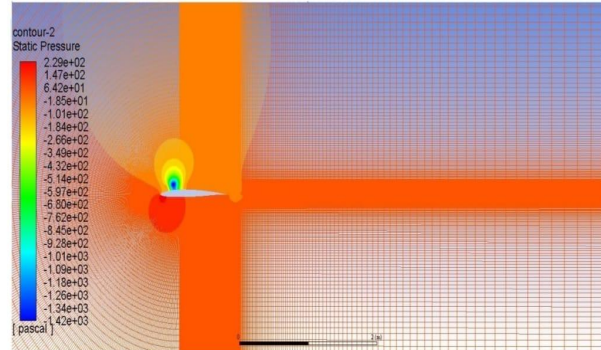


Fig 7 : Pressure analysis of RG-15

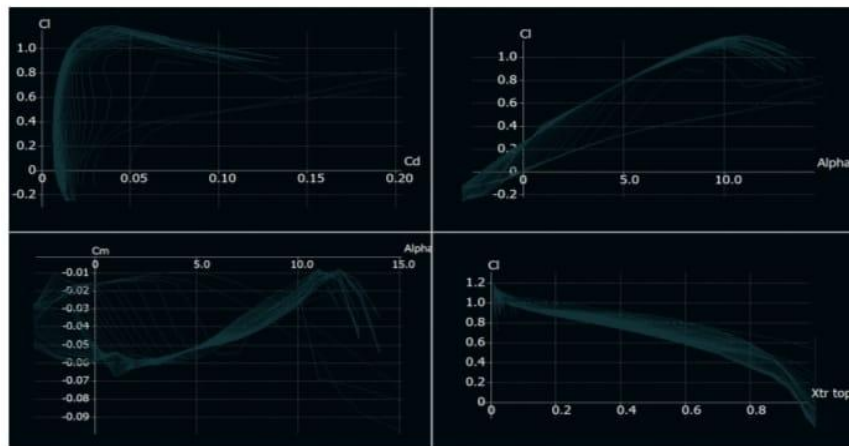


Fig 8 : Analysis of RG-15

### Morphed Wing:

Morphed wing configuration has been used for the UAVs fixed wings, which consists of three main components: **aluminum profiles, low-temperature foam, and silicone elastomers**<sup>[5]</sup>.

**Low-temperature foam:** It has been used to fill the gap between the aluminum profiles. A protective layer of low-temperature silicone elastomers has been applied to aluminum profiles and foam.

**Skin material:** Silica Elastomer has been used as the material for the skin hence making the morphed wing adaptable and flexible so that the material is handily twisted, while as yet having the solidarity to convey the streamlined loads of the UAV. Likewise, the material has been supplied with an abrasion resistance coating so that the material is not harmed when liable to evolving conditions. After the material has been converted to an alternate wing shape, the material recuperates its original size. The "skin" of the wing additionally

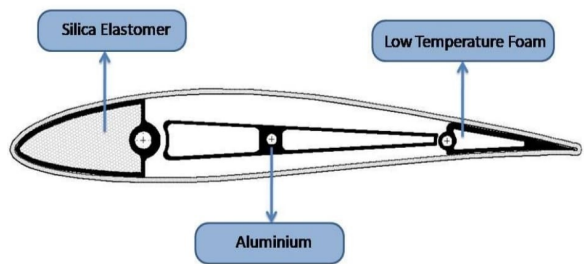


Fig 9 : Wing Structure And Material

Parameters	Morphed Wing
Root Chord	0.5 m
Tip Chord	0.3 m
Total Surface Area	1.2 m <sup>2</sup>
Span Length	3.6 m
Aspect Ratio	17.42

Table 2 : Fix Wing Parameters

upgrades the construction's exhibition. It has been produced using covering portions of adaptable material, layered to some degree like **quills or fish scales**, taking into account the pieces to get across one another as the wing flexes, while as yet giving a smooth external surface.

### UAV morphing plan:<sup>[6]</sup>

The plan will affect the flying performance of our UAV by the dramatic change of **wing shapes**. Such plans take out the requirement for various, costly, mission-explicit airfoils. Morphing airfoils can change their shape for various flying performances. Such changes can be either incremental changes to facilitate flight control. The key to the successful morphing of our wing was geometric scaling to match a particular performance requirement. The morphing would be carried out using 4 servo motors placed within the fixed wing and connected to the spars. These ensure precise morphing to facilitate the required aerodynamic characteristics.

### Tail Selection:

The Empennage provides for trim, stability and control and is designed to operate normally at only a fraction of lift potential. Y-Tail configuration has been chosen for reducing drag interference, avoiding the complexities of ruddervators, and keeping the propeller off the ground when compared to conventional tail. The horizontal tail provides better stability and vertical tail reduces aerodynamic sideslip and provides directional stability. NACA 0009, has been chosen for our UAV's tail which guarantees pitch control and longitudinal stability since it is a symmetrical airfoil. This airfoil also provides negative lift with an increased angle of attack, resulting in a negative moment, allowing the UAV to remain naturally stable.

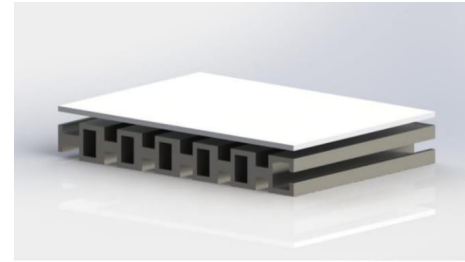


Fig 10 : Wing Surface

Parameters	Horizontal Tail	Vertical Tail
Root Chord	0.4188 m	0.25 m
Tip Chord	0.1637 m	0.15 m
Total Surface Area	0.74 m <sup>2</sup>	0.344 m <sup>2</sup>
Wing Span Length	2.5408 m	0.3 m
Wing Aspect Ratio	8.71	1.60

Table 3: Y tail design parameters

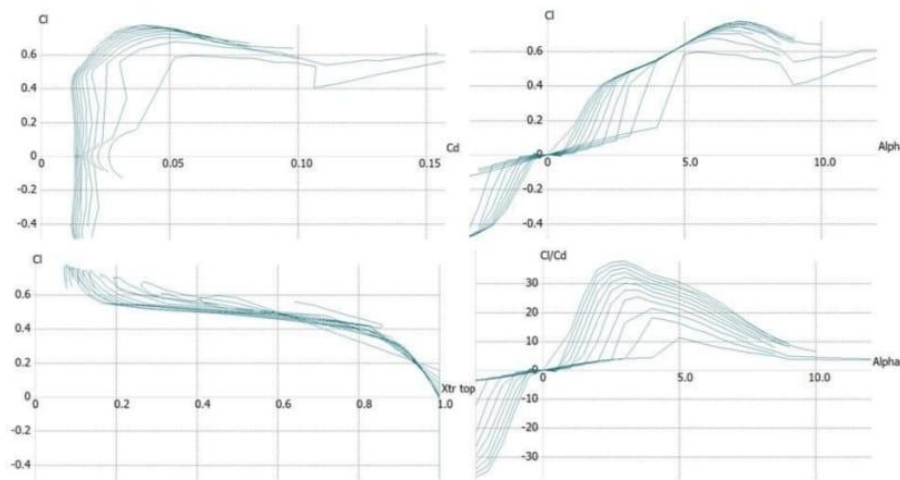


Fig 11 : Analysis of NACA 0009

## Propeller Design:

The propeller blade has been designed for the lowest weight possible. **Mylar** which is a light plastic material has been chosen to be used as the major component of the skin structure. Graphite epoxy composite [7] has been chosen as the material for the structure supporting the skin due to its high strength to weight ratio. A single hollow spar with rib structures to support the Mylar skin has been used as the baseline design. To prevent aeroelastic instabilities the center of gravity of the blade has been constrained to be coincident to the quarter chord axis location. **NACA 16-012** airfoil has been selected for our propeller. With a 70° twist angle and desired minimum thickness of 12%, our propeller ensures a high turning rate with a motor of (RPM).**3 blade design** is inherently smoother with reduced tip speed and minimal noise. This design marks constant thrust along the entire length of blades thereby maintaining the pitch to diameter ratio of 1:1 and making it more efficient.

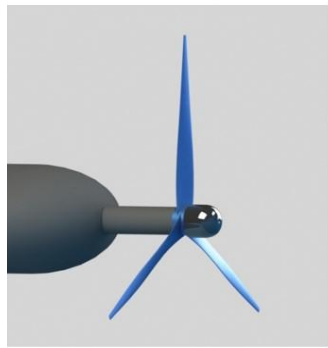


Fig 12: Propeller Design

## Payload Carrying Mechanism:

The mechanism that provides



Fig 14 : Docking Mechanism

certain degrees of freedom and hence relaxation in the codes to eliminate the need for precise alignment of the UAV and payload is undoubtedly the “**Stewarts Platform**” [8] also used widely in the space industry for docking space shuttles/ships onto the parent space stations. Therefore, inspired by this mechanism, a simple yet fail-proof payload-carrying mechanism has been designed for the safe retrieval of the payload. **The mechanism consists of two parts.**



Fig 13: Top View DS

## Passive Capture System:

The PCS is a modified Stewarts Platform working on three actuators connecting the upper and base lid. The actuators are released upon reaching the estimated location of the payload (within 20cm) and the upper lid is made to align with the payload. When experiencing high speed winds on Mars the UAV will be extremely unstable. In such circumstances to allow the locking system to continue, the actuators adjust accordingly. The base lid is equipped with three guide plates which slide into the slots made in the payload causing the rubber tubes to align. Upon alignment, the UAV is lowered in a controlled manner to apply pressure on the tubes in order to create a vacuum. This creates an upwards force preventing the box from falling. Hence the Passive Capture Phase is completed paving way for the Active Phase.



Fig 15 : PDM

## Active Capture System:

The Active Capture System is provided in case the PCS fails. It consists of three special motor-gear assemblies mounted on the base lid of the PCS which will lower three L-shaped rods. After the Passive phase completes, the actuators contract at an angle of 120 degrees w.r.t. each other which lifts the payload to a height of 10cm from the ground. Then the three L-shaped rods are lowered into slots made in the payload which are rotated by 180 degrees for good locking.

Hence the Locking sequence of the payload is completed.

## Payload Mechanism Control and Feedback:



Fig 17 : Payload

The actuators and motor have been controlled using a separate MCU unit (Microcontroller section). A closed feedback loop has been formed between the actuators/motor and the microcontroller. 12 Bit Absolute Positional Encoders working at 5V have been incorporated in every actuator and the motor. Since the ADC(Analog to Digital Convertor) present in the MCU has a resolution of 12 bit, the exact same value through a single line is received instead of using SSI (Synchronous Serial Interface) bus. Thus this Analog input signal closes the feedback loop from the actuators/motor to the MCU. A PID controller running in the MCU has been used to achieve accurate positions.



STEP 4: L-SHAPED RODS LOWERED INTO SLOTS  
STEP:4



STEP:5

Fig 16 : ADM

## Weight Distribution and Balancing:

The preliminary studies to estimate the weight breakdown have been carried out using the well-known **Boeing-Vertol** formulae. This utilizes size, gross weight, and other general specifications and fit this data to historical trends. Output from these formulae contain more specific weight information on subsystems of the UAV. The design has been optimised using the data so obtained in order to have a maximum scientific payload capacity without exceeding our weight estimates.

S.no.	Sub-System	Weight (kg)
1.	Structural	4.0
2.	Batteries and Propulsion	1.2
3.	Electrical	0.3
4.	Science Payload	4.7
	<b>TOTAL</b>	<b>10.2</b>

Table 4: Weight distribution

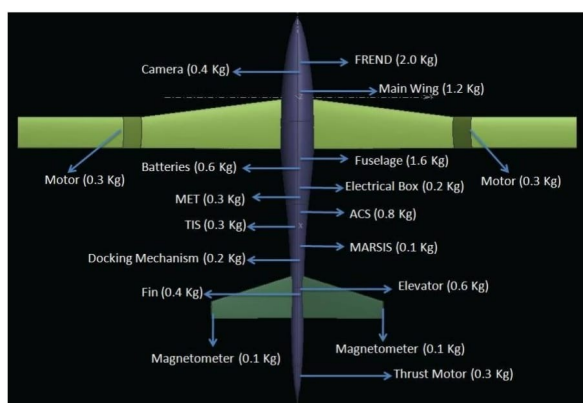


Fig 18 : Weight distribution

**Our final weight estimates slightly deviated from the traditional Boeing-Vertol formulae due to the following reasons:**

**1. Fuselage:** Our fuselage is lighter than predicted since our plane is unmanned. Composite materials have also been used throughout instead of traditional heavier metals.

**2. Wings and Blades:** Our wings and blades have been made using composite materials hence are lighter than traditional designs. Hence they were lighter than predicted.

## Environmental Control:

### Thermal Control System:

In order to make AVYAKT adaptable to the fluctuations in martian temperatures all the way from 20°C to a freezing -150°C we have introduced a wire meshing network in the main UAV body. The meshing is the primary heating system for the Electronics and Science subsystems. The network is connected to the centralized power system via a relay. The meshing is made of electrically insulating and thermally conductive diamond coating on Copper coils<sup>[9]</sup> thus providing electrical safety to the components without compromising on thermal parameters of the devices used.

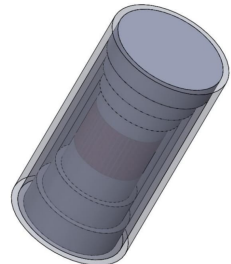


Fig 19 : RHU

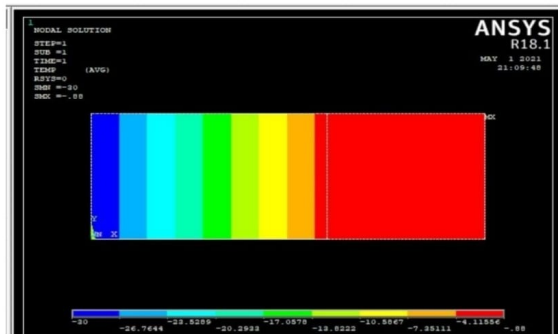


Fig 20 : Thermal analysis of Fuselage

In addition to the meshing network, a robust Temperature Control System(TCS) has been incorporated. The TCS is inclined towards sustainable temperature management without compromising any power consumption. It consists of 8 Radioisotope Heating Units (RHUs)<sup>[10]</sup> spread across the plane. RHUs have an excellent capability to produce heat and additionally provide the benefit of reduced electromagnetic interference to their electrical heating counterparts. It provides a constant supply of 1W heat without adding on a burden on the power cache as they provide heat through radioactive decay.

The placement of RHUs have been critical due to the difference in the amount of heat required by individual components. Adequate temperature range for each component is maintained using heat switches and insulation as discussed below.

**Heating module:** maximum heat insulation has been provided for the UAV to ensure it withstands cold Martian . All electronic components are placed within this insulated box known as Heating Module. It has been further thermally regulated using graphene tubings<sup>[11]</sup> perforated through the box which conduct heat through it to the base of the payload carrying mechanism. It prevents our UAV from overheating during operations on warm martian days.

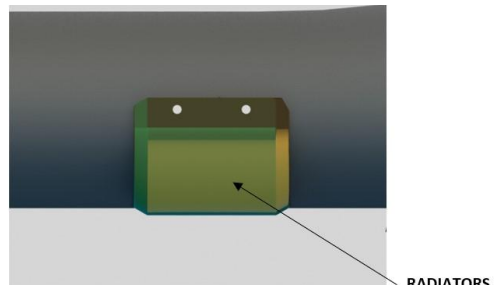


Fig 21: COPPER Radiators

**Shape memory heat switches<sup>[12]</sup>:** The radiators have been designed such that, in the worst scenario of temperature variation they maintain the optimal working temperature in the Heating Module. To prevent heat loss during the night, the conduction tubes would be connected to the radiator plates through Shape Memory Heat Switches. These are metallic materials that can return to a previous shape or size when subjected to the right thermal conditions. These switches can operate within a temperature range of roughly -200 C to +100 C, making them suitable for the martian atmosphere.



Fig 22: Heat Switch

To trap heat inside the UAV the inside of the UAV would be flushed with **CO<sub>2</sub> gas**. Also, a layer of **solid silica aerogel**<sup>[13]</sup> would be placed around the electronic box and the motors. Both carbon dioxide and silica aerogel are excellent insulators of heat. These prevent any unwanted heat loss from the plane's surface.

**Graphene** has been employed as the material for making the tubes as it has an excellent conduction and convection potential, hence making it an ideal material for making the tubes. To allow efficient heat transfer between radiators and the Martian atmosphere the radiators are made of copper which is an excellent conductor of heat.

### Dust Protection System:

Mars is infamous for intense dust storms, which sometimes kick up enough dust to be seen by telescopes on Earth. Individual dust particles on Mars are very small and slightly electrostatic, so they stick to the surfaces they contact and consequently the possibility of dust settling on and in machinery is a challenge for the mission. To prevent this from happening the entire exposed surface of the UAV is covered with a dust repellent layer of **CVD Nano-Coating**<sup>[14]</sup> that prevents the UAVs surface from wear due to the bombardment of fast-moving dust particles. To protect the cameras and lenses from damage due to dust and wind, they are equipped with lens-protective covers.

### Pressure Stabilizing System:

The mechanism comprises a lightweight two-stage pressure regulator that helps control the flow from a high-pressure source. Additionally, **High-Efficiency Particulate Absorbing (HEPA)** filters would be used to prevent dust from entering the UAV. This ensures that the internal pressure of the UAV remains equal to the external pressure.

### Power System:

Considering the flight time and the on board systems of the UAV, a robust power solution was required. The team was eager for a system which was self sufficient and would charge batteries efficiently for the flight. Also the constraints of weight posed a huge challenge for the system. Hence, Solar panels with Li-ion batteries have been finalized as the optimum solution.

### Solar Panels:

AVYAKT consists of solar cell technology with high efficiency solar cell designs, since only a limited amount of array area is available. The environmental conditions on the surface of Mars are quite different from the orbital environment in which space solar arrays normally operate. Some of the challenges in solar power<sup>[15]</sup> on Mars are:

- Lower Solar intensity due to greater distance from sun.
- Suspended atmospheric dust, which modifies the solar spectrum and reduces intensity
- Low operating temperatures

However, after research it was concluded that solar panels are still the best option if the panel has a large surface area while maintaining the weight constraints. The solar arrays are made up of triple-junction GaInP/GaAs/Ge Cells<sup>[16]</sup>.

Types of Solar cell	Maximum efficiency achieved
GaAs thin film	28.9 ± 1.0
Si Monocrystalline	22.9 ± 0.6
CdTe	17.5 ± 0.7
CIGS	15.7 ± 0.5
Si Thin film	8.2 ± 0.2

Table 5 : Efficiency of different Solar cell

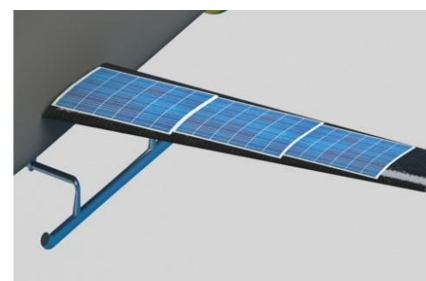


Fig 23: Solar Panels on Fixed Wing

Different approaches for solar panel arrays were considered including rollable and retractable solar wings but that mechanism would itself consume a decent amount of the power generated. Conventional panels were discarded as well, as they were less aerodynamically compatible with our design and were bulky. Thus, the idea of thin films originated. Our arrays have been set on the wings as well as the tail of the UAV in the form of thin film. These arrays cover an area of approximately 2 square meters. These solar arrays, on an average Martian day, can produce up to 200 watt-hour energy in clear weather conditions. This energy charged our batteries and was sufficient for 1 flight per sol.

### Dust Removal:

Settling dust may cause degradation in performance of a solar panel. To overcome this problem, we have implemented an **Electrodynamic Dust Shield**<sup>[17]</sup> for the removal of dust from the surface of panels. A

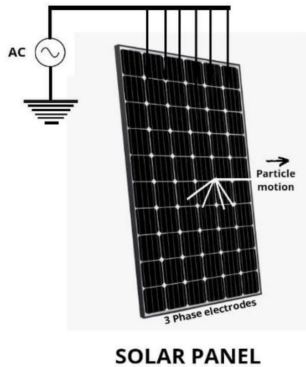


Fig 24 : Electrodynamic Dust Shield

series of parallel electrodes connected to AC source generates a traveling wave that acts as a contactless conveyor lifting and removing the dust particles from the panels. A pulsed AC output possesses the best dust removal capabilities. To decrease the breakdown potential, electrodes have been embedded in a transparent dielectric film. In this way, the surface was cleaned of particle deposition. The shield consists of parallel lines etched on a clad board. The surface of the shield has been covered with a thin layer of industrial grade polyurethane (PU). Thus the electrodes have been completely embedded in the highly resistive coating.

This system requires very less power when activated. On Mars, the system is activated only when dust removal is required, perhaps once a sol. Therefore, the daily power requirement has been relatively low.

### Charging:

The DC electricity generated by the solar panels is fed to the battery via a solar charge controller. Its job is to regulate the battery charging process. MPPT (Maximum Power Point Tracker) functions as an efficient DC to DC converter used to maximise the power output of a solar panel. The MPPT provides 30% more efficient charging and it forces solar panels to operate at voltage close to maximum power point to draw maximum power for operation and charging. MPPT also prevents batteries from getting overcharged, it stops or decreases the charging rate when the battery is fully charged. When the battery voltage drops below the cutoff voltage MPPT switch off the supply to the load which is known as Low Voltage Disconnect feature. This prevents the battery from permanent damage and increases life expectancy. Back feeding of batteries to solar panels at night is a major problem and thus MPPT prevents this to happen, hence, flattening the battery curve.

### Batteries:

For the operation of the UAV for the flight time of 10 minutes onboard batteries are a necessity. The

energy storage system on the rover consists of two lithium-ion rechargeable batteries each consisting of 10Ah Li-ion cells. The use of Li-Ion batteries, in place of conventional aqueous or alkaline systems, was primarily governed by the power and

Battery Characteristics	Silver Zinc	Lithium Polymer	Lithium ion	Nickel Cadmium	Nickel Hydride
Voltage per cell	1.2 to 1.85 V	3 to 4.2 V	2.5 to 3.7 V	1 to 1.4 V	1 to 1.4 V
Energy Density (Wh/Kg)	70-100	130-150	100-120	30-45	40-55
Shock Resistance	Good	Excellent	Good	Good	Fair
Cycle Life	10 –30 cycles	>500 cycles	>500 cycles	>1000 cycles	>800 cycles

Table 6 : Comparison between different types of Batteries

energy needs for the missions, within the constraints of mass and volume. The high energy density in Li-ion batteries means more power while not in a mission. The small size and the wide temperature range make the temperature management system inside the UAV easier.

### Betavoltaic Cells:

In accordance with the communication system requirement, we have used 3 betavoltaic cells<sup>[19]</sup> based on Nickel-63 having Nickel plating over it. These cells are lightweight and provide a constant voltage with a life expectancy of several sols. The foremost reason for choosing Ni-63 is because of its low radioactive nature, which reduces the risk of damage to other systems.

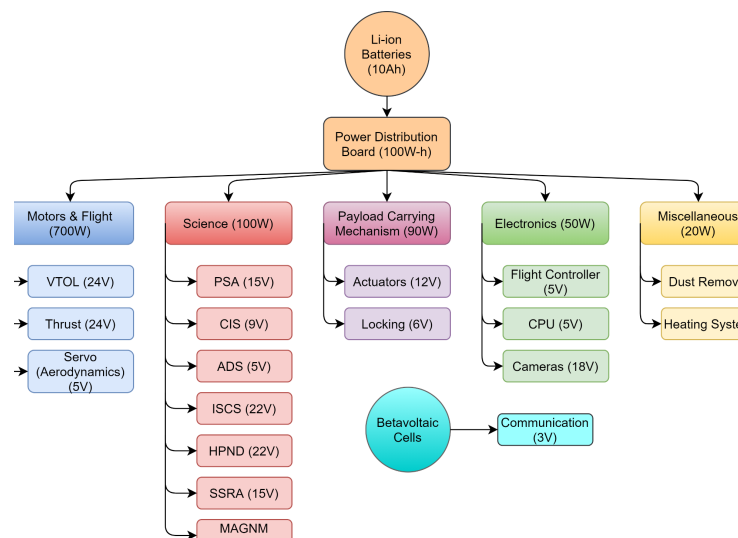


Fig 25: Power Distribution

### Power Distribution System:

The centralized battery system provides all the power for the flight. DC-DC converters are supposed to be providing power to the PM board controlled by the flight controller. The on board CPU and Dust removal system should be receiving independent powers via DC-DC and DC-AC converters respectively. The PM board is distributing the necessary power to each component via buses and FET (Field Effect Transistor) relays. Fault detection, isolation and correction of circuit boards are kept in mind before designing of the power bus. Power switching is accomplished with solid state FET relays. Load profiles drive PDS (Power Distribution System) design.

DC-DC converters isolated systems have been used on the power bus. Centralized power conversion is being used on small instruments. Peak Power Trackers (PPT) extract the exact power required from the solar array. The heating mesh has an independent supply from the batteries via a relay with temperature and fault detection mechanisms.

To ensure optimal battery condition, the batteries must not be discharged beyond 70% of their capacity. Discharging beyond this level will significantly reduce the health of the batteries. The batteries are connected to the Battery Monitoring System (BMS) which tracks the current health and charge of the batteries and sends the data to the CPU which further sends the data to the base station so that the flight team can keep a track of the charging.

### UAV Electronics:

The complete electronics sub-system has been designed to maximize efficiency while keeping the power consumption as low as possible and not compromising with the system's capabilities. As we know, the environmental conditions on Mars are too harsh for the electronic components used on Earth, like the low temperature of about -100 degrees Celsius at night, reduced aero-density, very weak ionosphere like layer in the atmosphere compared to Earth, etc. We have used general processors and other devices used on Earth but have ensured to enclose them thus, protecting them against radiation and maintaining optimum temperatures.

The UAV electronics broadly consists of the Flight Controller and CPU, which is the brain of AVYAKT, the mobility control (composed of the Power Managerial (PM) board and several Electronic Speed Controllers (ESCs)), various sensors for providing the environmental inputs, the vision, communication system and the power system. The figure presents a compact overview of the electronics system architecture inside the UAV. The following sections examine the presented architecture, and how the designed system presents solutions to the potential problems.

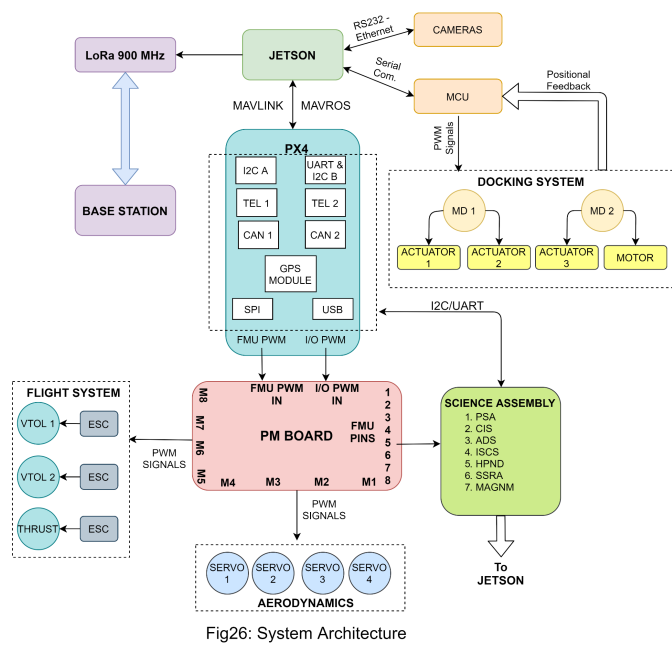


Fig26: System Architecture

processors for I/O and FMU (Flight Management Unit) operations which are further utilised for flight control and PWM (Main and Aux) output for motor/servos, Gimbal & other peripheral devices. It works easily in conjunction with the **Robot Operating System**. The embedded IMU in it as well as in built barometer for altitude detection are few of the many features of the PX4 autopilot which separate it from the rest of the flight controllers. It has **STM32F765** as the **main FMU processor** and **STM32F100** as the **IO processor**.

### Power Management (PM) Board with PX4:

PM board<sup>[22]</sup> is a dual purpose module working both as a power supplying module as well as power distribution board. It also provides the battery voltage and the current supply to the ESCs and servos connected to it. As pixhawk does not supply power to the servos, we require a 5V BEC (Battery Eliminator Circuit) connected to the positive rail supply and ground pins of the FMU based PWM pins on the power management board. The board provides ease in powering connections of ESC/servos and other peripheral devices and takes signal input from both I/O and FMU units. The input voltage ranges from 7 to 51V (2~12s LiPo).

### Motors:

Various parameters and constraints such as reduced atmospheric pressure, reduced gravitational force, 10 minutes of flight time and weight constraint were considered for assessing the required specifications and capabilities of the motors to be used.

### Central Processing Unit (CPU) :

The computer system on the UAV has been designed to achieve high dependability while keeping in mind the power aspects and efficiency of the system. The UAV contains 1.43 GHz Quad-core ARM A57 processor (NVIDIA Jetson Nano) with a 4 GB 64-bit LPDDR5 25.6 GB/s memory and a 128-core NVIDIA Maxwell architecture-based GPU. The GPU on the processor enables us to process images and implement various neural networks and machine learning algorithms on the UAV. A single processor can run on as little as 5 watts making it the best power efficient solution.

### Flight Controller:

The UAV is embedded with **PX4-Autopilot**<sup>[20][21]</sup> flight controller for the VTOL-fixed wing dual mode performance. It consists of separate

Thus, we required energy efficient, high RPM motors for the flight system. After exhaustively comparing the various technologies available, BLDC<sup>[23]</sup> (Brushless DC) motors came out to be on top, fulfilling almost all our needs. These motors provide us with the performance we need and can also be integrated in our system design with our ESC.

### Modes Of Operation:

The hybrid UAV consists of three modes<sup>[24]</sup> of operation with respect to flight stages. VTOL mode for vertical takeoff and landing along with inclusion of loitering as well at a specific altitude and location. The fixed wing aircraft mode for normal flight operations (horizontal translation). The transition and tuning mode for switching between VTOL and Fixed Wing mode.

Specifications	VTOL (24V)	THRUST (24V)
Type	Brushless DC Motor	Brushless DC Motor
% Throttle	75%	68%
Thrust (gf)	5500	3000
RPM	3000	3000
Current Rating	18A	12A

Table 7 : Motors Description

- 1) **VTOL mode:** This phase has been intended for vertical takeoff, landing and hovering operations. During this phase the outboard wing panels spin generating sufficient thrust in-order to lift the UAV. Rotor blades would be powered using two 24V VTOL motors. These motors, operating at 75% throttle, are capable of providing the required RPM and thrust. To minimize power consumption, after reaching the required altitude, the UAV platform immediately proceeds to flight in the aircraft mode. The two PWM enabled ESCs (connected to VTOL mode BLDC motor) signal wires connected to the PX4 autopilot FC are supposed to operate on 400 Hz, whereas the signal output to the ESC connected to the thrust motor must be zero along with the output to the servos connected to the wings.
- 2) **Transition mode:** The thruster mounted shaft of the UAV starts and provides a forward thrust. The two outboard wing panels are halted synchronously which causes a halt to the vertical motion of the UAV and the outboard panels now act as a fixed wing. With an increase in horizontal speed the fixed wings start to develop lift. When the transition occurs from VTOL to airplane mode, the signal output to ESC1 and ESC2 meant for VTOL operation is turned to zero and the output panels are locked for the fixed wing mode. The signal output to the ESC 3 along with the servos for frame movement is thus generated. Similarly when the transition occurs from fixed wing to VTOL the reverse occurs and the outboard panels start rotating.
- 3) **Aircraft mode:** During this phase, the UAV has attained sufficient speed of translational movement and is generating sufficient lift force counteracting its weight. Under such conditions the platform behaves like a conventional airplane and control surfaces such as ruddervators, ailerons, flaps provide the required yaw, pitch and roll motions are achieved using servos(5V, 2A). This phase is intended for energy efficient operation covering a major portion of the mission. The PWM enabled ESC signal wire connected to the PX4 for the thrust motor and the signal output to the servos would operate on 50 Hz.

### Microcontroller:

The payload carrying mechanism contains one 32 Bit STM32F7 Arm Cortex M7 core microcontroller with 8 MB of flash memory and 2560 KB of RAM packed inside the discovery kit. The 216 MHz MCU, with several I/O pins and communication buses, allows us to run components (run multiple subscribers and publishers on MCU) and reduce the processing load on the CPU. A single controller can run on a meagre power, making it adequately efficient for the UAV.

## Vision System:

A Navigation Camera has been used in conjunction with the PSA's camera instrument (discussed in further sections). This has been attached to the UAV, which is connected to the Jetson Nano and is controlled via MAVLink Messages. The Camera Feed can be streamed onto the Control Surface Interface via GStreamer Pipelines and a stripped-down version of QtGStreamer in order to support video streaming over UDP Ports. Video feed is received from the camera in H.264 Encoding and decoded by GStreamer and then used for Object Detection.

Specifications	
Rotation limits	360° Continuous Pan
IR sensor	SD 640x512 PIXEL /4X Digital Zoom
EO sensor	HD 1280x720 PIXEL /45X Optical Zoom
Additional features	Object Tracking Scene Tracking

The camera has high-definition electro-optics, high-sensitivity longwave infrared & an integrated inertial navigation unit. It offers excellent image quality and stabilization performance, making it an ideal solution for navigation and identification. The camera has 360° vision, a large field of view and is capable of capturing high definition images within a 15km radius.

Table 8: Payload Specifications

**Object Detection:** The Navigation Camera provides onboard image processing for object detection using the **YOLOv3<sup>[33]</sup>** algorithm, which combines feature extraction, object localization and classification into a single architecture for navigation and detection of grounded packages (as described in the Logistics Mission). The fact that all the detection and tracking is computed inside the camera itself ensures that the JETSON Companion Computer can run the software stack with efficiency and alacrity.

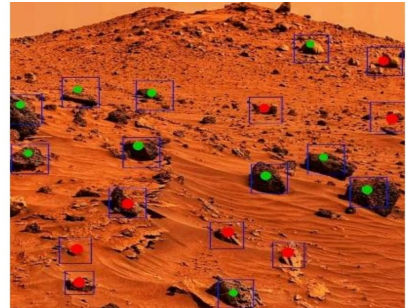


Fig 27 : Object Detection

**IMU:** PX4 has embedded **ICM-20689** and **BMI055** sensors. These sensors provide inertial measurements for measuring angular rates and accelerations in three perpendicular axes. The gyroscopes measure small heading changes very accurately and the accelerometers measure where the gravitational force is strongest. The magnetometer has been assumed to be operational on the basis of the magnetic field present in a specific region on mars.

ICM-20689	BMI055	IST8310	MS5611
6-Axis Motion Tracking Device	6-Axis Inertial Measurement Unit	3-Axis Magnetometer	Barometric Pressure Sensor

Table 9 : Embedded sensors in PX4

## Communication System:

The semi-autonomous control and time of flight of 10 minutes make it crucial to establish reliable and energy-efficient communication with the UAV. Considering the altitude reach of up to 10 Km and the radial range up to 5Km with an uncertain line of sight, a few modulation techniques have been considered and an exhaustive comparison has been performed as shown in the table given .

LoRa (Long Range) modulation technique based upon CSS technology (Chirp Spread Spectrum technology), primarily developed for ISM sub-GHz bands, turns out to be the most optimal solution because of its resilience

Attribute	Bluetooth® Low Energy Technology	Wi-Fi	Z-Wave	IEEE 802.15.4 (Zigbee, Thread)	LoRaWAN
Range (km)	0.01-1.5	0.015-0.1	0.03-0.05	0.03-0.1	2-20
Throughput	125 kbps – 2 Mbps	54 Mbps – 1.3 Gbps	10 kbps – 100 kbps	20 kbps – 250 kbps	10 kbps – 250 kbps
Power Consumption	Low	Medium	Low	Low	Low

Table 10: Comparison among Modulation Techniques

towards offsets, long range, better Bit Error Rate performance, relatively more straightforward demodulation, anti-interference superiority. Moreover, as energy conservation is an imperative criterion for such interplanetary missions, the low power consumption by the LoRa module in sleep, standby and idle mode minimizes power losses and makes it the obvious pick<sup>[25]</sup>.

The 400 MHz band is superior to the 915 MHz band in terms of range and signal attenuation, but the data transfer rates are low compared to the 915 MHz band. Since the 915 MHz fulfills our range requirement and has sufficient data transfer rates, it is the optimal choice as a continuous data transfer is required. For linking the UAV with the base station 2 LoRa module based nodes would be used, one on each. Both the nodes use a 19.6cm long, 1.3cm wide omnidirectional 915MHz ISM antenna with linear polarization (which provides an extended range). Following are the antenna's specifications as per the requirements : Impedance: 50Ω, Voltage Standing Wave Ratio: 1.75, and 12dBi peak gain<sup>[26]</sup>.

The antennas have been mounted perpendicularly on the nodes present on the UAV and at base station. The module present on the UAV directs the feed it receives from the various subsystems to the base station. The spreading factor adjusts accordingly to reduce the impact of the doppler's effect<sup>[27]</sup>.

## UAV Software:

The **PX4-Autopilot Framework** has been elected as the primary flight stack for the UAV due to its existing architecture developed for **Pixhawk** Flight Controllers, providing an expansive array of software with a host of practical services that can easily be manipulated. The operating system selected is **Ubuntu 18.04** due to the availability of several third-party software, packages, and services (like simulators and controllers), and the ease with which everything can be operated. **PX4 can properly work with ROS (Robot Operating System) only on Ubuntu 18.04.**

### ROS Wrapper:

The PX4 Framework, instead of being launched independently, is run via a **ROS Melodic Wrapper**. In this system, ROS acts as an Offboard API, creating another layer of communication between the base station and our UAV. Incorporating ROS allows us to use **ROS Nodes and Topics** for message transfer, which provides a broader scope of customization such that our own design can be easily controlled.

### Command System:

The **MAVLink (Micro Air Vehicle Link) Messaging Protocol** has been designated as the primary communication protocol between peripheral software and the drone, and **UORB** among onboard drone

components. UORB is the internal Publisher-Subscriber messaging system used for communication between interior modules.

MAVLink Messages are part of a hybrid Publisher-Subscriber structure combined with a P2P (Point-to-Point) system. Data is published as **Topics**, whereas configuration protocols are P2P Transfers with retransmission. This system allows easy integration of MAVLink Communication Systems into **ROS** via the **MAVROS Package**.

MAVROS essentially creates a MAVLink **ROS Node** and enables communication of Software with PX4 via a UDP Bridge. It also provides a plugin system to translate between ROS Systems and MAVLink Systems, allowing extremely straightforward methods to manipulate Parameters and Services.

### Simulators and Testing:

Another prominent merit of involving ROS in the software stack is the seamless incorporation of the **Gazebo Simulator**<sup>[28][29]</sup>. The UAV has been simulated in a host of scenarios with varying terrain and altitudes in Gazebo, using **PX4 SITL (Software-in-the-loop)**. Gazebo offers the ability to use custom terrains, obstacles, objects, and wind speeds, ensuring our UAV is well-equipped for the assigned missions. The **major limitation** of Gazebo, as is with all virtual simulations, is that its conditions may not be as challenging as the real world, causing the software stack to have to be ready for surprises.

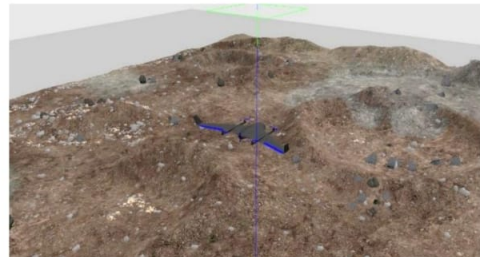


Fig 29 : VTOL Model flying in a Gazebo simulation of a Martian environment

### Control Surface:

The popular **QGroundControl** (QGC) has been used for waypoint-based flight control, and to provide an extensive, user-oriented interface for monitoring system status. Like most other peripheral software, QGroundControl communicates with PX4 over UDP Ports via MavLink Messages.



Fig 30 : Region Scan pattern on QGC

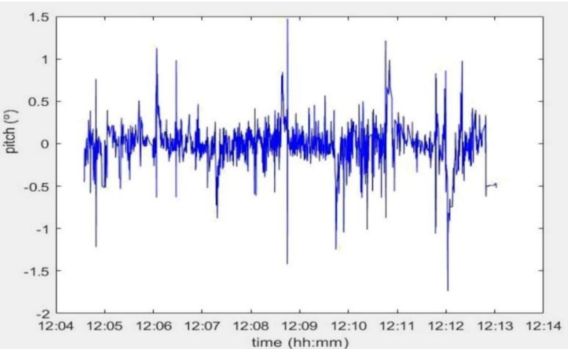


Fig 31: Pitch log after a mission on QGC

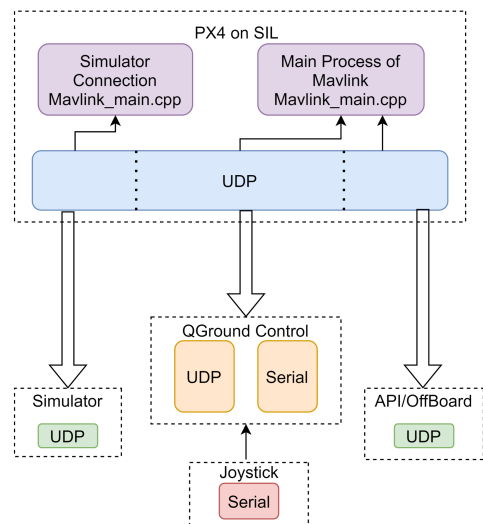


Fig: 28 Communication System Layout During Simulation

QGroundControl provides an inbuilt system for **Flight Planning**, allowing the operator to create and use complex, autonomous mission plans. Aside from an extensive array of flight patterns such as Surveys, Regions of Interest (**for locating objects in a specific region**), Loitering, Corridor Scans, and Structure Scans, it also incorporates other commands such as Remote Camera Triggering and Video Recording.

Another important feature of QGroundControl is the ease with which it provides a system for the monitoring and custom modification of PX4 Parameters alongside an efficient logging system and graphical displays of flight parameters (such as Pitch and Velocity).

### Autonomous Navigation and SLAM:

Simultaneous Localization and Mapping (SLAM), used to map the environment for collision avoidance, has been accomplished via **MonoSLAM**<sup>[30][31]</sup>, a lightweight SLAM Algorithm that uses Object Detection in our **Monocular Camera** (discussed in the Vision System Section) eliminating the need of exterior sensors like LiDARs or Multiple Cameras. MonoSLAM has been integrated with ROS using the **Mono-Slam Package**<sup>[32]</sup>. ROS Integration gives PX4 and QGC easy access to SLAM data, which can be used efficiently for Collision Detection/Avoidance, creating streamlined communication. **Rviz** has been utilized for effective Visualization of the **Point Cloud**.

QGC's **Flight Plan System** has been used for coordinate-based waypoint-oriented flight planning, with complex patterns and Camera Control, alongside QGC's **Object Avoidance Parameter** which allows SLAM to be seamlessly incorporated into our Flight Plan, tying our systems together to provide an overall autonomous, efficient, nimble & heavily-tested Software Stack.

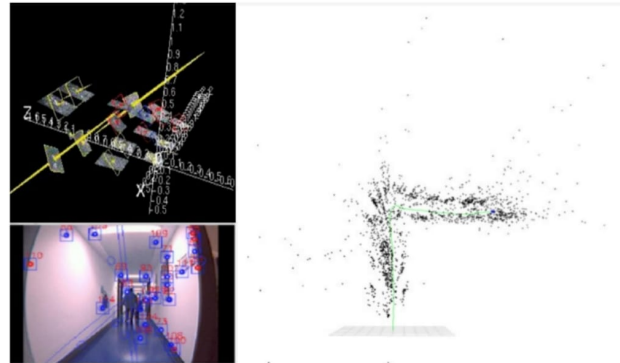


Fig 32 : Point Cloud generated by MonoSLAM

### Pre-Flight System Check:

The Pre-Flight Autonomous Check will consist of the following processes:

- All onboard sensors will begin monitoring the local atmosphere and the internal conditions of the UAV
- Heating and Pressure Control Systems will be tested and determined to be fully operational
- The motors will be activated and RPM will be measured using onboard sensors.
- Transmission and signal strength from the antennas will be measured.
- The orientation and stability of the UAV will be checked.
- Outboard flight panels will be rotated and their working will be ensured.

Once a full system check is performed, the UAV will start transmitting data to the base station, informing the mission control that it has been deployed successfully. The Rotor blades would then be spun up to their full RPM and a takeoff procedure would be initiated.

## UAV Science Package:

The majority of geologic evidence suggests that early Mars had a warm and dense atmosphere, possibly an ocean. Keeping all the requirements of the competition in mind the science module is designed to analyze the presence of life-supporting gases, soil patterns, the geology of the Martian surface.

### Planetary surface analyzer (PSA):

PSA is a CCD camera and electronics kit with a dual optical path and a single focal plane scope. It has a small physical size. The PSA instrument is intended for everyday summary, low-goal imaging of Mars to examine the advancement of climate frameworks and to notice changes in surface highlights caused by atmospheric changes. PSA's air examinations incorporate investigations of (1) the distribution of residue, condensates, and ozone in the climate. (2) the construction of condensate mists and their relationship to geography. (3) polar marvels. The camera works in five apparent and two bright (UV) groups and has a 180° field of view that grants perceptions of the planetary appendages.

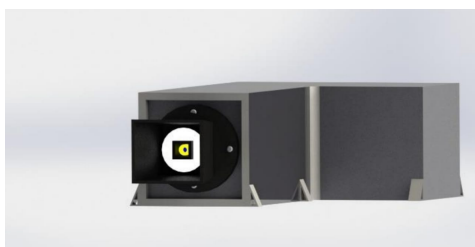


Fig 31 : Planetary surface analyzer( PSA)

PSA is placed at nadir orientation. To cover the desired wide spectral range of observation, the system consists of two separate sets of lenses and detectors for visible light images and ultraviolet images. A prism and parallel plate optical compensator align the lenses such that all wavelengths are imaged on a single focal plane array. A filter assembly made up of two fused silica plates bonded together is used by PSA. An opaque mask aids in the separation and suppression of the UV and VIS light paths. Every 2–3 seconds, the entire detector is readout.

The core of a central plane is a Charge Coupled Device detector of pixels 1024 × 9-mm. The digital signal processor (DSP) generates clocks at logic levels, which are then switched at the voltages required by the CCD using discrete P and N-MOSFET transistor pairs. CCD needs seven clock signals. Prior to amplification, a fixed DC offset is applied to carry the amplified signal into the 0–5 V range agreed by the ADC. The resulting AC-coupled signal covers half of the ADC range. An Analog to Digital converter digitizes the amplified CCD signal at its full rate of 3 Mpixels/sec to perform correlated double sampling and then subtracts in the digital domain for each pixel (CDS). Clock generation and sampling of the CCD signal are all handled by digital electronics. PSA uses a Modular Devices power converter to generate isolated +5 V and 15 V. The ripple on the 15 V is too much for the front-end video circuitry, so series-pass regulators are used to reduce it. Source-follower op-amps and Zener diodes provide the clock rail and DC bias voltages provided by the CCD. The DSP is in charge of generating CCD clocks, performing pixel processing, and transmitting data with Jetson is used as the central processing unit<sup>[34]</sup>.

### Caloric Imaging Spectrometer (CIS):



The Caloric Imaging Spectrometer is a plane reflection grating-based spectrometer which is used to detect emitted thermal infrared radiation from the Martian environment. Additionally, it would enable us to estimate the ground temperature of the surface of Mars and also map its surface composition like CO<sub>2</sub>, N<sub>2</sub>, Ar, O<sub>2</sub>, CO, H<sub>2</sub>O, Ne, Kr and Xe.<sup>[35]</sup>

Fig 32 : Caloric Imaging Spectrometer (CIS)

The general configuration of CIS is to focus ray into a slit at its focal plane using fore optics, a dispersing system which separates out different band, a collimating optics which collimates radiation from the slit, a focusing optical assembly which focuses different bands on to detector and a microbolometer DHA with camera electronics converts the thermal signal into an electrical signal (in terms of DN).

The important science goals of CIS are to estimate the global surface temperature, to study mineralogy and surface composition, to detect and study the variability of aerosol/dust along with the new spots indicating underground hydrothermal processes, and to check the variability of dust/atmospheric opacity of the Martian atmosphere. The study of aerosol turbidity in the atmosphere will help us to map the Martian weather, which could eventually help in planning the necessary flight plan according to Martian weather.

The analysis of CIS data involves the estimation of brightness temperature from thermal radiance data. It is followed by retrieval of surface temperature and emissivity spectra for various regions. The approach involves a theoretical modelling study using radiative transfer (RT) modelling within the thermal region at different atmospheric conditions of the Mars atmosphere. CIS hardware is provided with lightweight miniaturized components with a power requirement of 6 W along with a supply voltage of 9V.

### **Atmospheric Data System (ADS):**

The ADS package will provide the comprehensive measurements of the Martian near-surface atmosphere needed to fulfill the requirements of the atmospheric and climatic science goals of the mission [36]. The meteorology package includes sensors for wind, temperature, pressure, and humidity. The primary goals of this instrument are to characterize the weather, diurnal variations, carbon dioxide cycle, atmospheric saturation state, near-surface static stability, local dust raising capability, boundary layer structure, variations in near-surface water, the history of volatile reservoirs, and soil thermal properties to analyze conditions under which ground ice would be expected.

Wind speed and direction are measured by a nine-element hot wire array wind sensor and a two-element wind sensor together with the three fast thermocouple assembly temperature sensors. The temperature sensors are designed to provide reliable, time-resolved measurements of the atmospheric kinetic temperatures. The pressure sensor is a variable reluctance sensor that has excellent repeatability and reliability to work in extreme conditions.

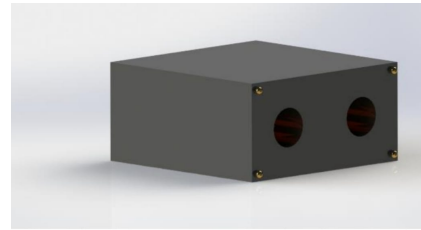


Fig 33 : Atmospheric Data System (ADS)

A tunable diode of 2.656 and 2.729-micron laser is mounted to measure the abundance of atmospheric water and carbon dioxide and to measure the isotopic ratios of carbon-13/carbon-12 and deuterium/hydrogen and oxygen-18/oxygen-16 in atmospheric water, and oxygen-18/oxygen-16 in atmospheric carbon dioxide. The TDL sensor measures water vapor concentrations by monitoring the level of absorption of a single vibration rotation line within the 1.37-micron water vapor band.

The voltage of the pressure sensor varies between 0 and 5 V and the voltage of the temperature sensor varies from -6.516 mV at 143.15K to +1.801 mV at 303K. The wind sensor has a voltage of 5V along with a power of 0.38W and a continuous current of 51.5 mA.

### Infrared Spectral Chemistry Suite (ISCS):

The primary goal of the ISCS instrument is to detect minor atmospheric gases along with sensitive detection of minor gases and isotopes to address global scientific problems related to Mars, such as volcanism, and climate evolution<sup>[37]</sup>. The investigations will be based on spectral analysis of solar radiation passed through the atmosphere, scattered by the atmosphere, and emitted by the atmosphere. The ISCS system consists of three different infrared spectrometers that share mechanical, electrical, and thermal interfaces.

The near-infrared channel (NIR), is a compact spectrometer designed to operate mainly in nadir and in solar occultation modes with a resolving power of  $\lambda/\Delta\lambda \sim 20,000$ . The scientific goals of NIR are the measurements of water vapor, aerosols, and dayside or night side airflow.

The mid-infrared channel (MIR) is a crossed dispersion echelle spectrometer equipped specifically for solar occultation measurements, with a resolving power of approximately 50,000. The spectrometer's large aperture, ultra-high spectral resolution, and efficient onboard frame processing ensure high efficiency.

The thermal-infrared channel (TIRVIM) is a double pendulum Fourier-transform spectrometer with solar occultation capabilities. Its primary mission is to profile temperature from the surface and to monitor aerosol abundance at nadir.

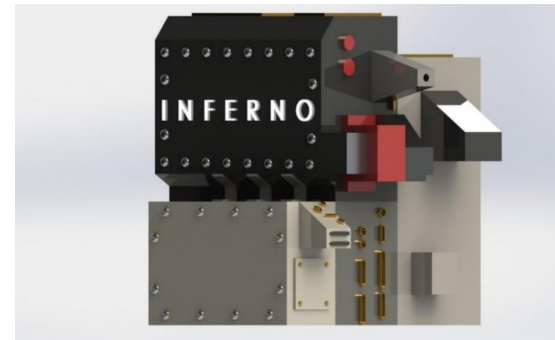


Fig 34 : Infrared Spectral Chemistry Suite (ISCS)

Channel Designation	Wavelength	Trace Gas Detected
Near- Infrared (NIR)	0.7 – 1.7 $\mu\text{m}$	$\text{H}_2\text{O}$ , $\text{O}_2$ , $\text{CO}_2$ , $\text{O}^{2-}$ , $\text{OH}^-$ , $\text{NO}$ -
Mid-Infrared (MIR)	2.2 – 4.4 $\mu\text{m}$	$\text{CH}_4$ , $\text{H}_2\text{O}$ , $\text{HO}_2$ , $\text{HDO}$ , $\text{HF}$ , $\text{HCl}$ , $\text{CO}$ , $\text{SO}_2$ , $\text{CO}_2$ and their isotopes, etc.
Far-Infrared (Thermal-Infrared) (FIR or TIRVIM)	1.7 – 17 $\mu\text{m}$	Temperature profiles, $\text{CO}_2$ , $\text{H}_2\text{O}_2$ , dust, water ice.

Table 11 : Trace Gas detection using ISCS

ISCS comprises a power board with DC/DC converters and a power switch, as well as a processor module board, a detector module, and control electronics, makeup. The electronics are physically separated from the thermal regulation systems. The processor module's Parallel Port Interface (PPI) is used to receive video data from the detector. UART0 and UART1 serial ports are used to control the detector as well as communicate with ISCS. The control Electronics module includes a microprocessor control system, a digitally controlled frequency synthesizer, and an RF power amplifier. The instrument consumes 30W of power at its peak during operation. The science channels are turned on by 22V lines.

### High Precision Neutron Detector (HPND):

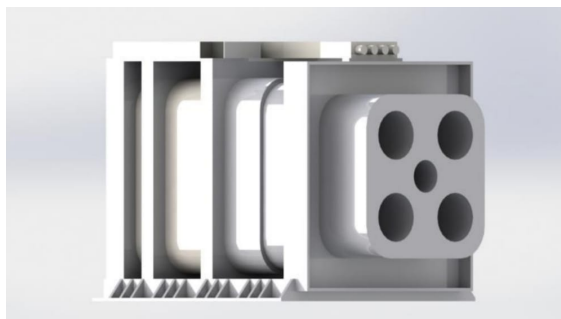


Fig 35 : High Precision Neutron Detector(HPND)

HPND is an orbital neutron telescope, designed for mapping the Martian neutron emission with high spatial resolution. The goals of HPND neutron mapping are :

- (1) Identifying local spots at equatorial and moderate latitudes with the highest groundwater content, then mapping and identifying these spots with relief features on the soil.
- (2) To calculate the difference in water content between the soil within craters and the soil surrounding them, and to analyze these differences in relation to the size and age of the craters.

(3) To address the northern and southern edges of water ice permafrost and equate these edges to shallow subsurface thermal properties.

(4) Assess the dynamics of seasonal carbon dioxide depositions on the ice, study the progression and regression of the edges during the fall-winter-spring transitions, and calculate the column density of depositions over the seasonal polar caps.

Along with a collimation module, the instrument will monitor the radiation environment and significantly narrow the field of view, thus allowing the creation of higher-resolution maps of hydrogen-abundant regions on Mars. The energy spectrum of leaking neutrons is a sensitive signature of hydrogen content in the soil, and this measured hydrogen content can be related to the presence of water <sup>[38]</sup>.

Technically, HPND can be divided into the following subsystems and modules: four <sup>3</sup>He proportional counters for epithermal neutrons with energies of 0.4 keV to 500 keV; one scintillation detector for high energy neutron detection; a high voltage (HV) provision subsystem and a digital electronics and thermal control subsystem. The instrument consumes 11.5W of power at its peak during operation and 7.5 W when on standby. The science channels are turned on by 22V lines.

### Subsurface Sounding Radar and Altimeter (SSRA):

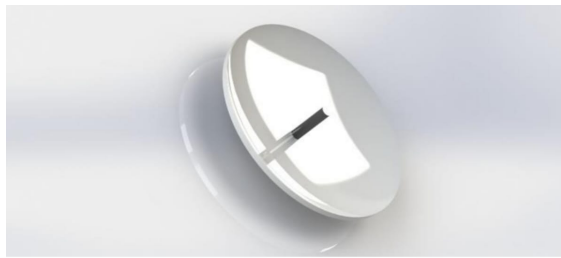


Fig 37 : Subsurface Sounding Radar and Altimeter

SSRA's primary goal is to map the distribution of water and ice in the upper layers of the Martian crust.<sup>[39]</sup> The instrument examines the radio wave reflections in the upper 2-3 Km of Mars' crust. It is able to distinguish between hot, frozen, and dry soil. SSRA extracts data on the electrical properties of the reflecting surface. It gives two different frequencies and analyzes the resulting echoes.

Radio waves are reflected by every surface they come into contact with. Due to the low frequency, a large portion passes through the crust. If there is a layer of liquid water, a radar echo is formed.<sup>[40]</sup>

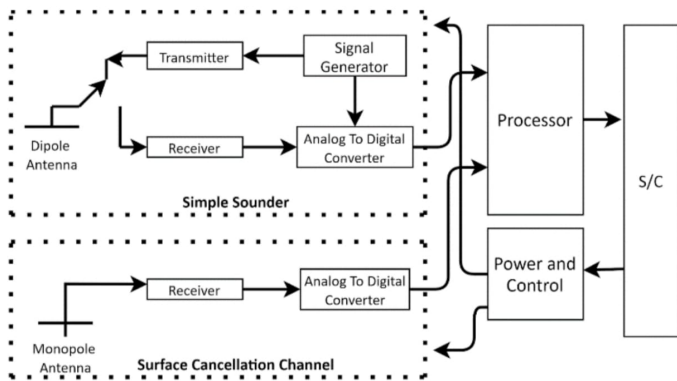


Fig 36 : SSRA Instrument Block Diagram

It uses a nadir-looking dipole antenna to transmit a linear frequency modulated chirp and a secondary monopole antenna to receive the return signal.<sup>[42]</sup> The SSRA<sup>[43]</sup> on-board digital processor formats the data and sends it to the main computer for further transmission. SSRA operates on a nominal 15 V input voltage and consumes about 30W of power.

### MAGNM Magnetometer:

The MAGNM magnetometer studies Mars' magnetic and electric fields, as well as its plasma environment and interactions with solar radiation<sup>[44]</sup>, to help explain why a planet once thought to have an abundance of liquid water became a frozen desert, which is crucial to understanding the character of solar radiation interactions with the planet.

The magnetic flux instrumentation consists of two independent triaxial magnetometer sensors, remotely mounted at the outer extremity of the y-tail of UAV systems. The magnetometer uses a series of coils, each with a magnetic ring wrapped around a metal core, to measure the magnetic flux on Mars. Magnetic fields are used to drive the sensors, known as "flux gates," in and out of saturation. The sensors remain balanced if there is no ambient field.

If there is an ambient field present, the sensors will become saturated in one direction quicker than the other. The presence of an ambient field is revealed by the imbalance.

Each magnetometer measures the vector field of surroundings over a large dynamic range. The magnetometer helps us see where the atmosphere is protected by mini-magnetospheres and where it's open to solar radiation, which might help us to form a much bigger picture of the planet's overall atmosphere.

Magnetometer sensors are placed as far away from spacecraft subsystems as possible to reduce the relative contribution of spacecraft-generated magnetic fields and to take full advantage of the  $1/r^3$  diminution of a magnetic (dipole) source with distance. A pair of magnetic sensors provides hardware redundancy as well as the ability to detect magnetic fields at two different locations on the spacecraft. By comparing the magnetic fields measured by each sensor, this capability has the potential to keep track of spacecraft-generated magnetic fields.

SSRA comprises the antennas, the RF equipment (transmitter and receivers), and the digital electronics. The receivers and digital electronics are housed together in a separate package. It is regulated by the Digital Electronics Subsystem (DES). Data is stored in frames, which are blocks of data. Each frame is long enough to produce a synthetic aperture at the frame's lowest frequency. Initial echoes may be collected to train the radar for frame acquisition. The instrument can make measurements in 1 MHz wide bands centered at 1.8, 3.0, 4.0, and 5.0MHz<sup>[41]</sup>.

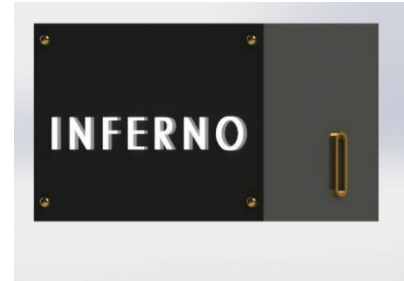


Fig 38 : MAGNM

The sensors are controlled by independent and functionally identical electronics assemblies that are integrated within UAV subsystems and draw their power from redundant power supplies within that system. The magnetometer electronics require a voltage of 13 V for optimal operation. Local linear regulators are used in the Magnetometer electronics to generate the required internal voltages for the analogue reference voltage. To confirm extra safety, shielded connectors are accustomed to connecting magnetometers with the CPU.

---

## REFERENCES:

1. Robert L. Fusaro; "**Lubrication of Space Systems**".
2. William J. Fredericks; "**Conceptual design of a VTOL Unmanned Aerial Vehicle with 24Hr Endurance**"
3. Wolf Elber; "**Toughening of Graphite-Epoxy Composites by Interlaminar Perforated Mylar Films**"; NASA March 1978.
4. California State University Northridge; "**Project Ares II: High-Altitude Battery Powered Aircraft**"; Proceedings of the NASA/USRA Advanced Design Program 7th Summer Conference.
5. Oliver Schorsch, Andreas Luhring, Christof Nagel et al. ; "**Polymer Based Morphing Skin for Adaptive Wings**".
6. Hangil You, Seongik Kim et al.; "**New Concept for Aircraft Morphing Wing Skin: Design, Modeling and Analysis**". DOI: 10.2514/1.J058102
7. Rudy Lukez; "**The use of Graphite/Epoxy Composite Structures in Space Applications**".
8. Michael Hardt, Jose Ramon Villa, Daniel Cocho et. al.; "**Simulation and Control of an Active Stewart Platform for Docking and Berthing of Space Vehicles**". January 2006
9. **Diamond-like carbon coating** for effective electrical insulation of Cu and Al wires, Daichi Nakajima, Hiroki Kuwabara.
10. NASA Article on "**Radioisotope Heater Unit**".
11. Yifeng Fu; "**Graphene related materials for thermal management**" et al 2020 2D Mater. 7/01/2001.
12. K. Lankford; "**Heat Switches**" Starsys Research Corporation, Boulder Colorado.
13. J.E. Fesmire; "**Aerogel Insulation Systems for Space Launch Applications**."
14. A. Delfini, A. Vricella, R. Bueno Morles. "**CVD nano-coating of carbon composite for Space materials.**" Procedia Structural Integrity Volume 3, 2017.
15. Geoffrey A. Landis, Thomas W. Kerslake, Phillip P. Jenkins and David A. Scheiman "**Mars Solar Power**", Second International Energy Conversion Engineering Conference sponsored by the American Institute of Aeronautics and Astronautics Providence, Rhode Island, August 16–19, 2004.
16. D. Crisp, A. Pathare, R.C. Ewell, "**The performance of gallium arsenide/germanium solar cells at the Martian surface**", Acta Astronautica, Volume 54, Issue 2, 2004.
17. R.A. Sims, A.S. Biris, J.D. Wilson, C.U. Yurteri, M.K. Mazumder, C.I. Calle and C.R. Buhler "**Development of a Transparent Self Cleaning Dust Shield for Solar Panels**", NASA Kennedy Space Center.

18. B. V. Ratnakumar, M. C. Smart, L.D. Whitcanack, R. C. Ewell and S. Surampudi; “**Li-Ion Rechargeable Batteries on Mars Exploration Rovers**”.
19. Young RangUhm, Byoung GunCho,i Kwang JaeSon “**Study of a Betavoltaic Battery Using Electroplated Nickel-63 on Nickel Foil as a Power Source**”.
20. **PX4 Autopilot** <https://px4.io> .
21. **Pixhawk Hardware Designs** <https://github.com/pixhawk/Hardware>.
22. “**Pixhawk 4 Wiring Quick Start:Power Module (PM07)**” [https://docs.px4.io/master/en/assembly/quick\\_start\\_pixhawk4.html](https://docs.px4.io/master/en/assembly/quick_start_pixhawk4.html)
23. Hedlund, “**Motor system design for large UAV**” Dissertation, 2017.
24. Roman Czyba, Marcin Lemanowicz “**Construction Prototyping, Flight Dynamics Modeling, and Aerodynamic Analysis of Hybrid VTOL Unmanned Aircraft**” Journal of Advanced Transportation, Hindawi 2018.
25. Augustin, Aloës; Yi, Jiazi; Clausen, Thomas; Townsley, William M. 2016. "A Study of LoRa: Long Range & Low Power Networks for the Internet of Things" *Sensors* 16, no. 9: 1466.
26. Afar Communications;” **RF Link Budget Calculator**” <https://afar.net/rf-link-budget-calculator/>.
27. A. Rahmadhani, Richard, R. Isswandhana, A. Giovani and R. A. Syah, "LoRaWAN as Secondary Telemetry Communication System for Drone Delivery" 2018 IEEE International Conference on Internet of Things and Intelligence System
28. García, J., Molina, “**J.M. Simulation in real conditions of navigation and obstacle avoidance with PX4/Gazebo platform**”. *Pers Ubiquit Comput* (2020).
29. J. Zhu and C. Xu, "A comprehensive simulation testbench for aerial robot in dynamic scenario using gazebo-ros" 2017 Chinese Automation Congress (CAC), 2017, pp. 7664-7669, doi: 10.1109/CAC.2017.8244165.
30. Russo, Ludovico & Rosa, Stefano & Bona, Basilio & Matteucci, Matteo. (2014). “**A ROS Implementation of the Mono-Slam Algorithm**”. Computer Science & Information Technology. 4. 339-351.
31. Y. Chen, N. González-Prelcic and R. W. Heath, "Collision-Free UAV Navigation with a Monocular Camera Using Deep Reinforcement Learning" 2020 IEEE 30th International Workshop on Machine Learning for Signal Processing (MLSP), 2020, pp. 1-6.
32. A. J. Davison, I. D. Reid, N. D. Molton and O. Stasse, "MonoSLAM: Real-Time Single Camera SLAM" in IEEE Transactions on Pattern Analysis and Machine Intelligence, vol. 29, no. 6, pp. 1052-1067, June 2007.
33. Joseph Redmon, Ali Farhadi, “**YOLOv3: An Incremental Improvement**” in ArXiv in Computer Vision and Pattern Recognition, April 2018

34. Wolff M., Malin M., Calvin W. "**Mars Reconnaissance Orbiter Mars Color Imager (MARCI): Instrument description, calibration, and performance.**" *The Journal of Geophysical Research Planets*.
35. R. P. Singh, Somya S. Sarkar, Manoj Kumar, "**Thermal Infrared Imaging Spectrometer for Mars Orbiter Mission**".
36. Park, Y.H.. (2000). "**Mars Volatiles and Climate Surveyor (MVACS)**".
37. Korablev, O. & Montmessin, F. "**The Atmospheric Chemistry Suite (ACS) of Three Spectrometers for the ExoMars 2016 Trace Gas Orbiter.**" *Space Science Reviews*.
38. Mitrofanov, I. & Malakhov, A. "**Fine Resolution Epithermal Neutron Detector (FREND) Onboard the ExoMars Trace Gas Orbiter**". *Space Science Reviews*.
39. Jordan, Rolando & Picardi, G. (2009). "**The Mars express MARSIS sounder instrument**". *Planetary and Space Science*.
40. Mars Express: "**Instrument Design Marsis**"  
<https://sci.esa.int/web/mars-express/-/31033-objectives?fbid=longid=658>
41. Mars Express: "**Instrument Objectives Marsis**"  
<https://sci.esa.int/web/mars-express/-/34826-design?fbid=longid=1601>
42. Seu, R., et al. (2007), **SHARAD sounding radar on the Mars Reconnaissance Orbiter**, *J. Geophys. Res.*, 112, E05S05,
43. **Mars ozone measurements from the Mars Reconnaissance Orbiter (MRO) MARCI and CRISM experiments**, in Seventh International Conference on Mars, July 9 – 13, 2007, Pasadena CA [CD-ROM], LPI Contrib., 1353, Abstract 3082.
44. Connerney, J.E.P., Espley, J., Lawton, P. et al. "**The MAVEN Magnetic Field Investigation**". *Space Sci Rev* 195, 257–291 (2015).